EARTHQUAKE ENGINEERING AND STRUCTURAL DYNAMICS
Earthquake Engng Struct. Dyn. 2011; **40**:807–825
Published online 17 November 2010 in Wiley Online Library (wileyonlinelibrary.com). DOI: 10.1002/eqe.1061

Prediction and validation of sidesway collapse of two scale models of a 4-story steel moment frame

D. G. Lignos[1,*,†,‡], H. Krawinkler[1] and A. S. Whittaker[2]

[1]*Department of Civil Engineering, Stanford University, Stanford, CA 94305-4020, U.S.A.*
[2]*Department of Civil, Structural and Environmental Engineering, The State University of New York, University at Buffalo, U.S.A.*

SUMMARY

A research program is summarized in which collapse of a steel frame structure is predicted numerically and the accuracy of prediction is validated experimentally through earthquake simulator tests of two 1:8 scale models of a 4-story code-compliant prototype moment-resisting frame. We demonstrate that (1) sidesway collapse can occur for realistic combinations of structural framing and earthquake ground motion; (2) $P-\Delta$ effects and component deterioration dominate behavior of the frame near collapse; (3) prediction of collapse is feasible using relatively simple analytical models provided that component deterioration is adequately represented in the analytical model; and (4) response of the framing system near collapse is sensitive to the history that every important component of the frames experiences, implying that symmetric cyclic loading histories that are routinely used to test components provide insufficient information for modeling deterioration near collapse. Copyright © 2010 John Wiley & Sons, Ltd.

Received 16 February 2009; Revised 11 June 2010; Accepted 14 June 2010

KEY WORDS: sidesway collapse; component deterioration; $P-\Delta$ effects; scale model; collapse prediction; deterioration model; loading history

1. INTRODUCTION

Difficulties in predicting collapse of building frames with high confidence have been an impediment to the implementation of performance-based earthquake engineering. Although more attention has been focused in the past decade on the limit state of incipient collapse, the triggers for collapse are not well established and robust constitutive models for components through failure are not yet available. This paper seeks to fill some of these gaps in our knowledge, with a focus on steel moment-resisting frames.

A significant number of analytical studies on the topic of collapse prediction have been carried out in the past. In most studies it is acknowledged that modeling of deterioration is a critical aspect of collapse prediction. Various analytical models have been developed to capture stiffness and strength deterioration. Foliente [1] summarized the use of the Bouc–Wen model [2, 3] and its derivatives to account for component deterioration [4, 5]. Sivaselvan and Reinhorn [6] developed a versatile smooth hysteretic model that includes stiffness and strength degradation and pinching, derived from inelastic material behavior but based on the earlier models by Iwan [7] and Mostaghel [8]. More recently, Ibarra *et al*. [9] proposed a component deterioration model that

*Correspondence to: D. G. Lignos, Department of Civil Engineering, Stanford University, Stanford, CA 94305-4020, U.S.A.
†E-mail: dlignos@stanford.edu
‡Post-Doctoral Fellow.

has been implemented in various studies concerned with collapse prediction of frame and wall structures [10–12].

Much less work is reported in the literature on experimental validation of analytical models and physical tests to collapse. Vian and Bruneau [13, 14] performed a series of earthquake simulator tests of 15 SDOF steel frame models subjected to earthquake excitations of progressively increasing intensity up to collapse. They concluded that the stability coefficient $P\delta/Vh$ (P is the vertical load, δ is the story displacement, V is the base shear, and h is the story height) had a significant effect on the behavior of single degree-of-freedom (SDOF) systems close to collapse. The work by Vian and Bruneau was confirmed by Kanvinde [15] after performing earthquake simulator tests of similar SDOF frames. Using the Open System for Earthquake Engineering Simulation Platform (OpenSees [16]) Kanvinde showed that collapse of SDOF systems due to $P-\Delta$ effects can be reproduced analytically. But deterioration was not an issue in these studies because the inelastic components of the steel frame models were of rectangular cross-section.

The consequences of beam-to-column connection fractures on the global behavior of steel moment-resisting frames were investigated through a series of shaking table experiments and numerical simulations by Rodgers and Mahin [17]. Based on experimental and numerical investigations, they demonstrated that severe strength loss due to a combination of numerous fractures, undesirable post-fracture hysteretic behavior, $P-\Delta$, and large earthquake excitations can cause a structure to experience large residual drifts or collapse.

Tests through collapse of a full-scale steel 4-story building designed to current Japanese seismic provisions were conducted recently at the E-Defense earthquake simulator in Miki, Japan [18, 19]. The objective of the test series was to enhance analytical methods for earthquake response simulation and provide information for new design guidelines for collapse assessment of steel structures. In these tests, deterioration in strength and stiffness of tubular columns contributed significantly to collapse. Many pre- and post-test predictions have been reported in the literature (e.g. [20, 21]), but detailed experimental results of these tests are not yet available to the public.

The research project described in this paper sought to expand our knowledge on collapse prediction for steel moment-resisting frames by explicitly addressing $P-\Delta$ effects and component deterioration. The existing numerical tools were refined on the basis of component tests and then validated by earthquake simulator testing of two steel moment-resisting frames.

2. MODELING OF FRAME STRUCTURES FOR COLLAPSE PREDICTION

Our work focused on the refinement of deterioration models to enable the prediction of collapse of planar bare steel moment-resisting frames. We acknowledge that these analytical models alone are not sufficient for collapse predictions of buildings because factors such as torsion, biaxial bending of columns, beam–column panel zone deformations, composite action of floor slabs and steel beams, inadequate column splices and contributions to strength and stiffness from the gravity–load-resisting system and non-structural components are not considered in the analytical models.

2.1. Modeling of deterioration at component level

The accurate prediction of collapse of frame structures under earthquake shaking requires the development of versatile models that include rules for stiffness and strength deterioration (e.g. [6, 9]). We used a modified version of the Ibarra–Krawinkler (IK) deterioration model [22] for this purpose. The phenomenological IK model, which is shown in Figure 1, is based on a backbone curve that defines a boundary for the behavior of a structural component and establishes strength and deformation bounds, and a set of rules that define the basic characteristics of the hysteretic behavior between the bounds. Cyclic deterioration is quantified using a deterioration parameter that is based on a reference energy dissipation capacity of the component defined as $E_t = \Lambda \cdot M_y$, where Λ is a property of the component [9, 22]. Up to four modes of cyclic deterioration are defined with respect to the backbone curve. Details of this deterioration models are presented in [22].

DOI: 10.1002/eqe

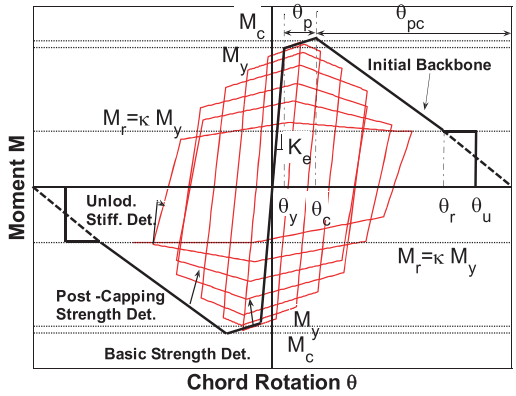

- Effective yield strength and rotation (M_y-θ_y)
- Effective stiffness $K_e = M_y/\theta_y$
- Capping strength and associated rotation for monotonic loading (M_c, θ_c)
- Pre-capping plastic rotation for monotonic loading θ_p
- Post-capping rotation θ_{pc}
- Residual strength $M_r = \kappa \cdot M_y$
- Ultimate rotation capacity θ_u

Figure 1. Modified IK deterioration model; backbone curve, basic modes of cyclic deterioration, and definitions.

To better understand the importance of deterioration of component strength and stiffness on collapse predictions for steel moment-resisting frames, we first used experimental data from more than 300 components tests [22, 23] to calibrate the parameters of the deterioration model summarized in the preceding paragraph. We used this empirical model to judge whether component data collected using traditional cyclic loading protocols could be used to predict the response of a frame through collapse, recognizing that component deformation histories in buildings responding to earthquake shaking are different from the symmetric pattern employed in traditional loading protocols.

2.2. Modeling of structures

Beams and columns in the analytical and physical models employed in this study are represented by elastic elements with point plastic hinges at the ends. The point hinges are represented by rotational springs, whose properties are intended to represent all inelastic moment–rotation characteristics of flexural components (concentrated plasticity model). In the analytical model, deterioration properties of the rotational springs are idealized by the modified IK model discussed in Section 2.1. In the physical model, plastic hinge elements of the type described in Section 5.2 are utilized. In the analytical model, joint panel zones are modeled with the parallelogram model discussed in [24]. In the prototype structure summarized in Section 4 the panel zones were designed with sufficient strength to respond elastically. This simplified the design and fabrication of the physical model, since the story drift caused by panel zone shear deformations could be incorporated by modifying the elastic stiffness properties of the beam and column elements. In both the analytical and physical models the second-order $P-\Delta$ effects are modeled with a 'leaning column'. In the physical model (test frame) discussed in Sction 5.2 the leaning column is represented by an arrangement denoted as mass simulator. Composite slab action and the contributions of the gravity system to lateral strength and stiffness are not considered.

3. OVERVIEW OF ANALYTICAL EXPERIMENTAL STUDY

The components of the research program addressed in this paper are as follows:

(1) Design of a 4-story steel moment-resisting frame structure based on the current seismic provisions that can serve as the prototype for analytical predictions and experimental validation.
(2) Design and fabrication of two 1:8 scale model frames whose properties represent those of the prototype as closely as can be achieved at this model scale, and which are tested to collapse. The scale was dictated by fabrication constraints and the size of the Network

DOI: 10.1002/eqe

for Earthquake Engineering Simulation (NEES) earthquake simulator facility at the State University of New York at Buffalo (SUNY-UB).

(3) Performance of two series of component experiments. The first series is performed prior to the execution of the Buffalo earthquake simulator tests and is used to calibrate the component deterioration model on which pre-Buffalo collapse predictions are based. The term *pre-Buffalo* is used to identify experiments and analytical predictions performed prior to the earthquake simulator tests. The second series of component experiments is performed after the execution of the earthquake simulator tests and serves to improve the deterioration models by considering the deformation history experienced by the components in the earthquake simulator tests.
(4) Pre-Buffalo prediction of the inelastic response of the scale model of the prototype steel moment-resisting frame under a series of ground motions of increasing intensity.
(5) Execution and evaluation of earthquake simulator tests of two 1:8 scale models of the prototype frame, using the ground motions employed in the pre-Buffalo predictions.
(6) Post-Buffalo prediction of the inelastic response till collapse, taking advantage of the improved deterioration models obtained from calibrations based on the post-Buffalo component experiments.
(7) Assessment of differences in pre-Buffalo and post-Buffalo predictions.

4. PROTOTYPE STRUCTURE

The 4-story building shown in plan in Figure 2(a) serves as the prototype building for this project. The structural system of this building is designed for vertical and lateral loads in accordance with the design provisions of the 2003 IBC [25] and AISC [26] for a site in Los Angeles area assuming soil type D. The structural system is a special moment-resisting frame (SMRF) with reduced beam sections (RBS) designed per FEMA-350 [27]. The first story is 4.6 m (15 ft.) in height; all other story heights are 3.7 m (12 ft.). A992 Grade 50 steel is used for all structural steel components. The seismically effective weight is 4.6 kN (1050 kips) for each of the first three floors and 5.3 kN (1200 kips) for the roof (to account for a penthouse). Our focus is on the east-west (EW) framing. The EW moment-resisting perimeter frame is shown in Figure 2(b). The first three modal periods in this direction are 1.32, 0.39, and 0.19 s, respectively. Columns are assumed to be fixed at their base. All columns are spliced at the mid-height of the third story. The drift limits, which control the sizes of the beams and columns, are based on the predominant period of the structure from computer analysis as permitted by IBC [25]. The building frame is symmetric and the orthogonal framing systems are uncoupled, which permits testing of one moment frame only and sets aside the need to consider biaxial loading effects of columns.

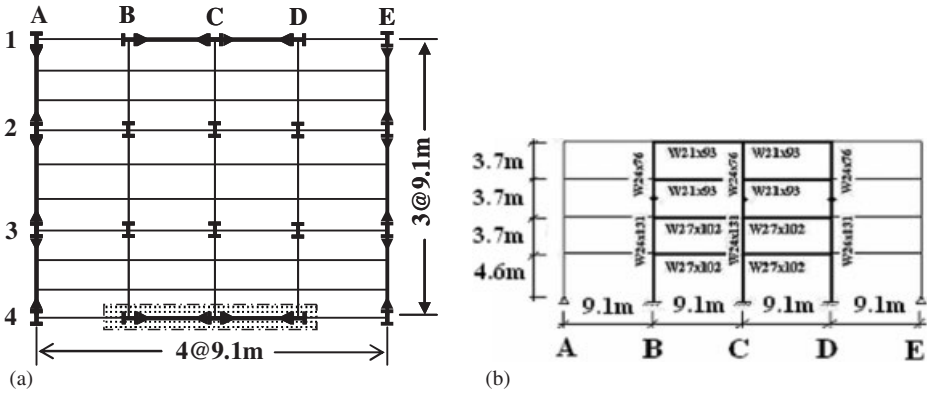

Figure 2. 4-story prototype structure; (a) plan view and (b) elevation on line 4.

DOI: 10.1002/eqe

5. DESIGN AND FABRICATION OF 1:8 SCALE MODEL TEST FRAMES

An important part of this research project was the planning, design, fabrication, erection, and testing of two scale model test frames on the NEES earthquake simulator at the University at Buffalo. Each test frame was a 1:8 scale model of the prototype 4-story EW moment-resisting frame shown in Figure 2(b). At this scale, the total reactive weight assigned to the EW frame is approximately 40 kips (e.g. [28]) and within the capacity of the simulator to collapse the frame.

Significant effort was spent determining how to best support the masses and gravity loads of half of the building, since the latter are required for simulating sidesway collapse. In the analytical model, gravity load effects can be placed on a leaning $P-\Delta$ column. In the physical model, two sub-structures are used: (1) the scale model of the SMRF in the EW direction (denoted as the model frame, see Figures 3(a) and (b)), and (2) a mass simulator (see Figure 3(a)). The two sub-structures are connected with near-rigid links in the horizontal direction at each floor level to transfer inertia forces and $P-\Delta$ effects from the mass simulator to the test frame (see Figure 3(b)). Each link is equipped with a load cell and an articulated joint (hinge) at each end. Figure 3(a) illustrates both sub-structures after erection on the earthquake simulator, with the test frame to the left and the mass simulator to the right. More information regarding erection process can be found in [22].

5.1. *Test frame and plastic hinge elements*

The test frame, which is shown in Figure 3(b), consists of an elastic beam and column elements and elastic T- or cruciform-shaped joints, joined by plastic hinge elements. The elastic elements are aluminum, and proportioned to properly simulate element stiffness based on similitude rules [28]. The test frame geometry is shown in Figure 4(a). The configuration and details of the plastic hinge elements installed in the test frame is the product of an extensive component testing program that is discussed in Section 6. The challenge is to develop an element that (1) is easy to fabricate and assemble, (2) can be installed at all possible plastic hinge locations in the test frame, and (3) can simulate deterioration of strength and stiffness of the plastic hinge regions of the prototype beams and columns at all levels of deformations up to collapse.

A typical plastic hinge element, which is shown in Figure 4(b), consists of a spherical hinge (rod-end bearing) whose function is to transfer shear force, two steel flange plates that are machined from bar stock so that flexural plastic hinging (with appropriate deterioration) at the ends of beams and columns is realistically represented at model scales, spacer, and clamping plates that permit adjustment of the distance between the flange plates and of the buckling length of the flange plates, which is controlled by the distances L_t and L_b (see Figure 4(b)), and four bolts that are post-tensioned after all plastic hinge elements are installed and the test frame is carefully aligned. These plastic hinge elements are inserted at the ends of all beam and column elements of the model test frame, recognizing the possibility of inelastic behavior at all these locations.

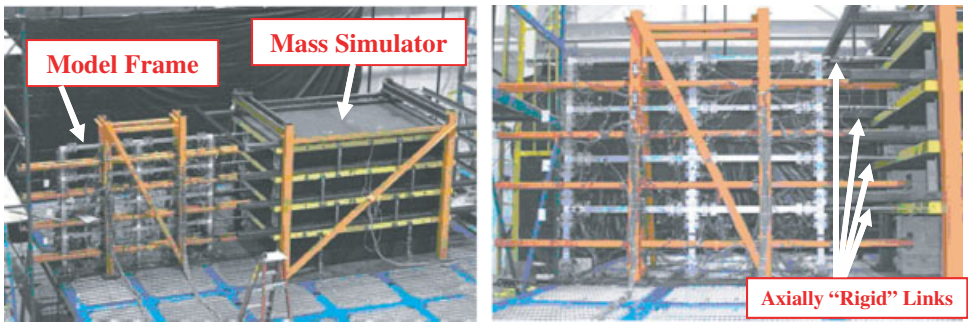

Figure 3. Four-story scale model and mass simulator on the SUNY-Buffalo NEES earthquake simulator: (a) aerial view and (b) elevation of test frame.

DOI: 10.1002/eqe

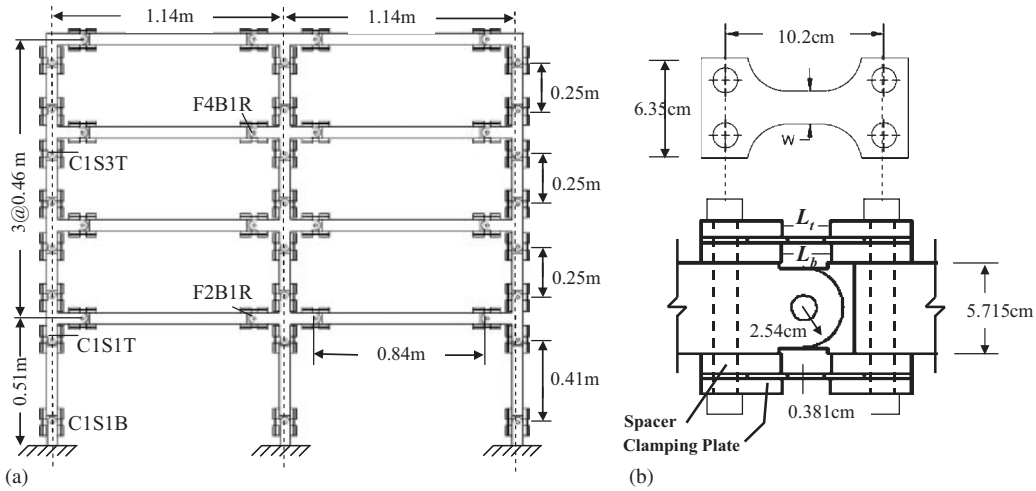

Figure 4. Test frame geometry and typical plastic hinge element: (a) frame elevation showing plastic hinge elements and (b) plastic hinge control parameters.

Two test frames (Frame 1 and Frame 2) were constructed. Frame 2 is nominally identical to Frame 1. The elastic beam and column elements used in Frame 1 were re-used in Frame 2. All flange plates of the plastic hinge elements in Frame 1 were replaced for the testing of Frame 2. Identical flange-plate geometries and materials were used in the two frames.

5.2. Mass simulator and test frame-to-mass simulator links

Four steel plates of almost identical weight available in the laboratory at the University at Buffalo are used to simulate gravity loads (one plate per floor). The plates, which are approximately $3 \times 2 \times 0.09$ m ($118 \times 79 \times 3.5$ in.), are connected with four vertical links per story. Each vertical link has a spherical hinge at each end to permit free rotation. It is a mechanism that has no lateral resistance when disconnected from the test frame. The mass simulator is connected to the test fame with horizontal links at every floor level, forcing the test frame and the mass simulator to undergo equal horizontal displacements at every floor level, which is necessary for properly simulating $P-\Delta$ effects. The four links are instrumented to act as load cells to provide accurate measurement of story forces applied by the mass simulator to the test frame, including $P-\Delta$ effects.

5.3. Lateral bracing and safety systems

The test frame and mass simulator are supported laterally to eliminate out-of-plane motion because the earthquake simulator testing program was designed to subject the frame to unidirectional loading only. Figure 3 shows the lateral-restraint systems used for the test frame and the mass simulator. The restraint frames also serve to protect the earthquake simulator in the event of a catastrophic failure or excessive story drift. Timber blocks are placed between the plates in the mass simulator to prevent the steel plates from collapsing onto the simulator below. Lignos and Krawinkler [22] provide a detailed description of the lateral bracing and safety systems.

5.4. Instrumentation

A total of 314 and 247 transducers are used to record the response of Frames 1 and 2, respectively. Accelerometers are used to record the absolute acceleration of the floors of the test frame and the mass simulator to compute story and base shears. The flange plates of the plastic hinge elements are strain gauged to (1) trace initiation of yielding at plastic hinge locations, (2) record how plastification of critical plastic hinge elements progresses based on the clip gage and strain gage measurements, and (3) provide moment and shear force measurements in the elastic range. Aluminum clip gages are employed to measure the flange plate elongation during each test. These

DOI: 10.1002/eqe

gages are custom-made extensometers to monitor the behavior of a flange plate over a 3.80 cm (1.50 in.) length from elastic behavior up to fracture. Displacement transducers include linear potentiometers and a Krypton 3D recording system, which is used to monitor the displacement response of the simulator platform, test frame and mass simulator, and rotations at the selected plastic hinge locations. The data recorded from all instruments in all tests performed on the Buffalo earthquake simulator are available from the NEES repository http://nees.org/resources/723.

6. PRE-BUFFALO COMPONENT EXPERIMENTS

A series of 50 component tests are undertaken prior to the earthquake simulator tests to identify (1) the appropriate configuration of the plastic hinge elements (2) the dimensions of flange plates for each plastic hinge element, (3) the geometry and boundary conditions required to replicate the hysteretic behavior of the prototype connections, and (4) the deterioration characteristics of each component of the test frame.

The goal for configuring and detailing the plastic hinge elements is to simulate at the model scale the moment–rotation relationships of the beams and columns used in the prototype structure (Figure 2(b)). No attempt is made to accommodate the influence of composite floor slabs. A typical calibrated moment–rotation plot obtained from a full-scale component with RBS tested by Uang *et al.* [29] is presented in Figure 5(a). The plot illustrates that strength deterioration commences

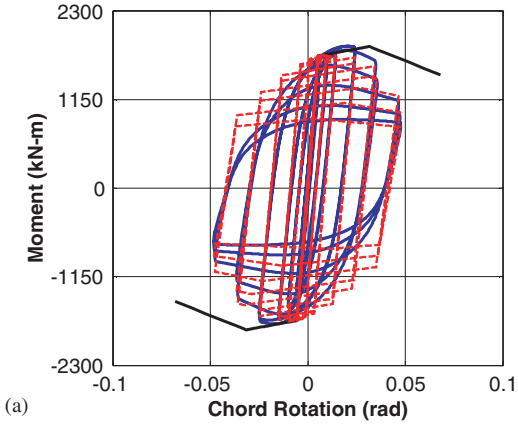

(a)

(b)

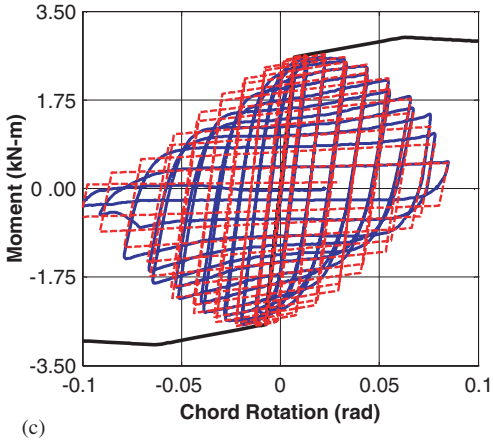

(c)

Figure 5. Component testing program: (a) typical hysteretic behavior of $W30 \times 94$ beam with RBS similar to the one used in the EW moment-resisting frame of prototype structure (data from [29]); (b) test apparatus; and (c) calibrated $M-\theta$ diagram.

DOI: 10.1002/eqe

Table I. Modeling parameters of plastic hinge elements for pre-Buffalo collapse prediction.

Location	Width w (cm)	M_y (kN m)	K_e (kN m/rad)	M_c/M_y	θ_p (rad)	θ_{pc} (rad)	Λ	κ
C1S1B*	3.40	3.73	2924	1.09	0.05	1.3	1.35	0
C1S1T†	2.80	3.06	2331	1.1	0.05	1.3	1.35	0
C1S3T‡	1.47	1.61	1265	1.1	0.05	1.3	1.35	0
F2B1R§	2.11	2.15	1469	1.1	0.05	1.3	1.35	0
F4B1R¶	1.47	1.5	1265	1.1	0.05	1.3	1.35	0

*C1S1B: Column 1 in Story 1 at Base.
†C1S1T: Column 1 in Story 1 top location.
‡C1S3T: Column 1 in Story 3 at top.
§F2B1R: Floor 2 Beam 1 right location.
¶F4B1R: Floor 4 Beam 1 right location.

at a chord rotation of about 2% and becomes severe at 4%. Information about the deterioration characteristics of the prototype components are presented in [22] and are not repeated here.

Fifty component tests are carried out to establish the plastic hinge details. The following important dimensions of the flange plates and boundary conditions are varied systematically: L, w, d, L_t, and L_b. Figure 4(b) is a drawing of the plastic hinge element. All flange plates are 0.381 cm (0.15 in.) thick and of ASTM A572 Grade 50 steel. The width w in the reduced region is varied to meet the strength demands at each potential plastic hinge location in the test frame. This width is listed in Table I for the five plastic hinge element sizes identified in Figure 4(a). Specimens with single and double plate arrangements are tested both monotonically and cyclically, using a Universal Testing Machine at the Stanford University and the test setup shown in Figure 5(b).

Typical recorded (solid line) and calibrated (dashed line) moment–rotation diagrams of a component sub-assembly with two steel plates, using the AISC loading protocol [26], are shown in Figure 5(c). The pre-Buffalo response predictions for both test frames are based on deterioration model parameters obtained from these component tests. The models are calibrated mostly from tests with symmetric cyclic loading histories supplemented by a few monotonic tests. The backbone curve is based on the monotonic curve of the plastic hinge element and the cyclic deterioration parameter Λ is calibrated to the value that the computed and experimental moment rotation diagram is matched well (see Figure 5(c)).

A comparison of test results obtained from the model plastic hinge elements with those of prototype beam elements (see Figures 5(a) and (c)) shows that reproduction of prototype deterioration characteristics is not at all perfect, which could not be avoided because the plastic hinge elements cannot undergo web local buckling or lateral torsional buckling that are generally associated with RBS connections at large rotations. Table I summarizes the calibrated deterioration parameters of the modified IK model used for the five plastic hinge elements of the numerical model for the pre-Buffalo response predictions.

7. EARTHQUAKE SIMULATOR TESTING PROGRAM AND PRE-TEST PREDICTIONS

The earthquake simulator testing programs for Frames 1 and 2 used earthquake shaking of increasing intensity through collapse. The selected intensities are intended to represent those of interest to the profession: service-level earthquake (SLE), design-level earthquake (DLE), maximum considered earthquake (MCE), collapse-level earthquake (CLE). For Frame 1, one ground motion record is used for all intensities. The fault normal (FN) component of the Canoga Park (CP) record of the 1994 Northridge earthquake is selected for this purpose because its elastic response spectrum provides a good match to the design spectrum for the prototype structure in the vicinity of its first mode period (see [22]). The 5% damped spectrum of the CP record is shown in Figure 6 together with the design spectrum used for the prototype design. The CP record is scaled by a factor of 0.4, 1.0, 1.5, and 1.9, respectively, to represent the SLE, DLE, MCE, and CLE levels. The scale

DOI: 10.1002/eqe

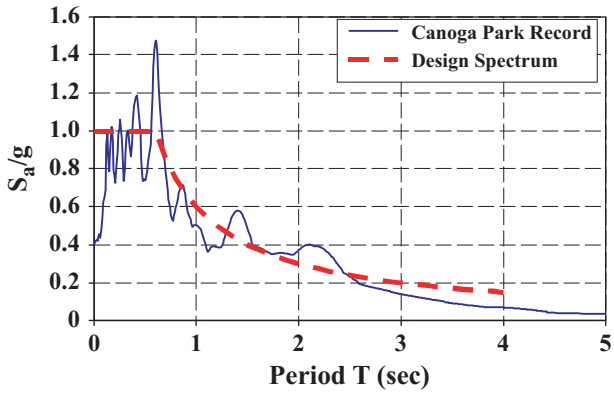

Figure 6. Design-level spectrum and acceleration spectrum of the fault normal component of the 1994 Canoga Park earthquake record.

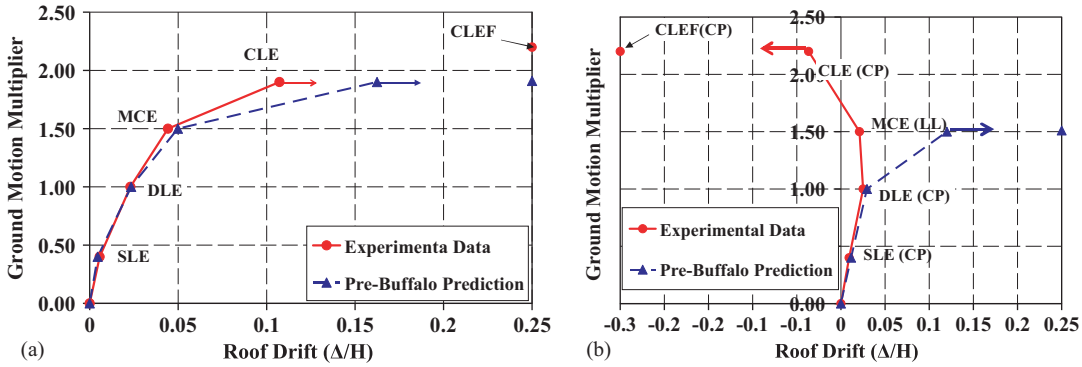

Figure 7. Pre-Buffalo predictions of frame response and selected experimental data: (a) Frame 1 and (b) Frame 2.

factor of 0.4 is selected for the SLE level because this intensity of shaking brings the frame to the point of yield. The scale factor of 1.5 for MCE shaking is taken directly from the IBC. The scale factor of 1.9 for CLE shaking is based on pre-Buffalo predictions as being sufficient to trigger collapse.

The response for all levels of interest is predicted from a computer analysis of the scale model in which all beams and columns are modeled as elastic elements connected by rotational springs that represent the plastic hinge elements discussed previously. The strength, stiffness, and deterioration properties of these rotational springs are based on calibrations obtained from the pre-Buffalo component experiments and are summarized in Table I. A modified version of the analysis program Drain-2DX (Prakash *et al.* [30]) is employed for the response predictions. The maximum roof drifts predicted at the four intensity levels of interest are shown as dashed lines in Figure 7(a) for Frame 1. A roof drift ratio (Δ/H) of 0.17 is predicted for the CLE shaking. Although collapse is not predicted at this intensity of shaking, the scale factor of 1.9 is selected for the CLE level to learn more about structural response close to collapse and to challenge the prediction models and tools. Residual deformations from the previous testing phase were used as initial conditions to the next prediction.

For Frame 2, the CP record is used for SLE and DLE shaking. The fault normal component 10 of the Llolleo record of the 1985 Chile earthquake is used for the MCE shaking to assess response to an earthquake with different frequency contents and strong-motion duration. The Llolleo (LL) record has a long duration of strong motion, which is expected to produce larger cumulative damage and earlier deterioration in component response than the CP record. The pre-Buffalo predictions

DOI: 10.1002/eqe

for Frame 2 are shown as dashed lines in Figure 7(b) and indicate that at the MCE level, at which the Llolleo record is employed, the structure is expected to be close to collapse. The reason why the experimental MCE drifts are so different from the analytical pre-Buffalo predictions is that the earthquake simulator failed to reproduce the LL record at the MCE intensity. For this reason we switched back to the Canoga Park record using a scale factor of 2.2 to represent a collapse level earthquake.

The test sequence for frames constituted a *physical* Incremented Dynamic Analysis [31] with the residual conditions at the end of one test forming the initial conditions for the following test.

8. BUFFALO EARTHQUAKE SIMULATOR TESTS—RESULTS AND EVALUATION

This section presents the selected salient results obtained from the earthquake simulator tests. A detailed evaluation of the tests is provided in [22]. All data presented here are in the model domain. For conversion to the prototype domain, length quantities should be multiplied by 8, force quantities should be multiplied by 64, and time should be scaled by $\sqrt{8}=2.83$.

8.1. Modal properties

A series of white noise (WN) and sine–sweep (SS) tests are conducted to identify the modal properties of the two test frames. Figure 8 shows the first two mode shapes of Frame 2 obtained by measurement (experiment) and eigenvalue analysis [32].

The first and second mode periods of Frame 2 are 0.46 and 0.16 s, respectively, which matches well with the scaled modal periods of the prototype frame. The accurate quantification of equivalent viscous damping was not possible because of friction damping in the support linkages of the mass simulator, which made the equivalent viscous damping ratio dependent on the amplitude of response. The friction damping arises from friction in the rod-end bearings and could not be eliminated. The equivalent viscous damping ratio was about 3% in the first mode based on large-amplitude WN and SS tests. In the post-Buffalo response predictions, the effect of friction damping was incorporated by inserting rotational friction dampers at the ends of the $P-\Delta$ leaning columns in each story. Friction damping was found to affect the response significantly at SLE shaking but not at higher intensities of shaking [22, 33].

8.2. Global behavior of test frames

Experimental data are superimposed (solid lines) on the pre-Buffalo predictions in Figure 7. The roof drift histories (relative displacement of the roof with respect to the base) for the two test series are shown in Figure 9. Only the segments of large amplitude motion for each test are presented.

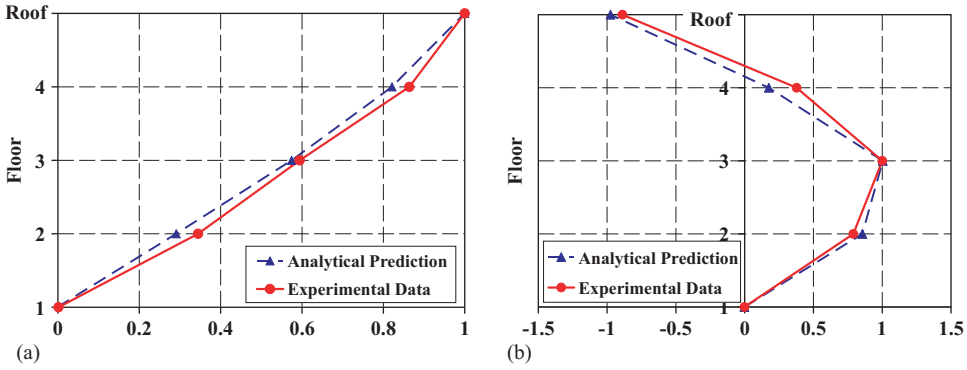

Figure 8. Modal properties of Frame 2: (a) first mode, $T_1=0.47$ s and (b) second mode, $T_2=0.13$ s.

DOI: 10.1002/eqe

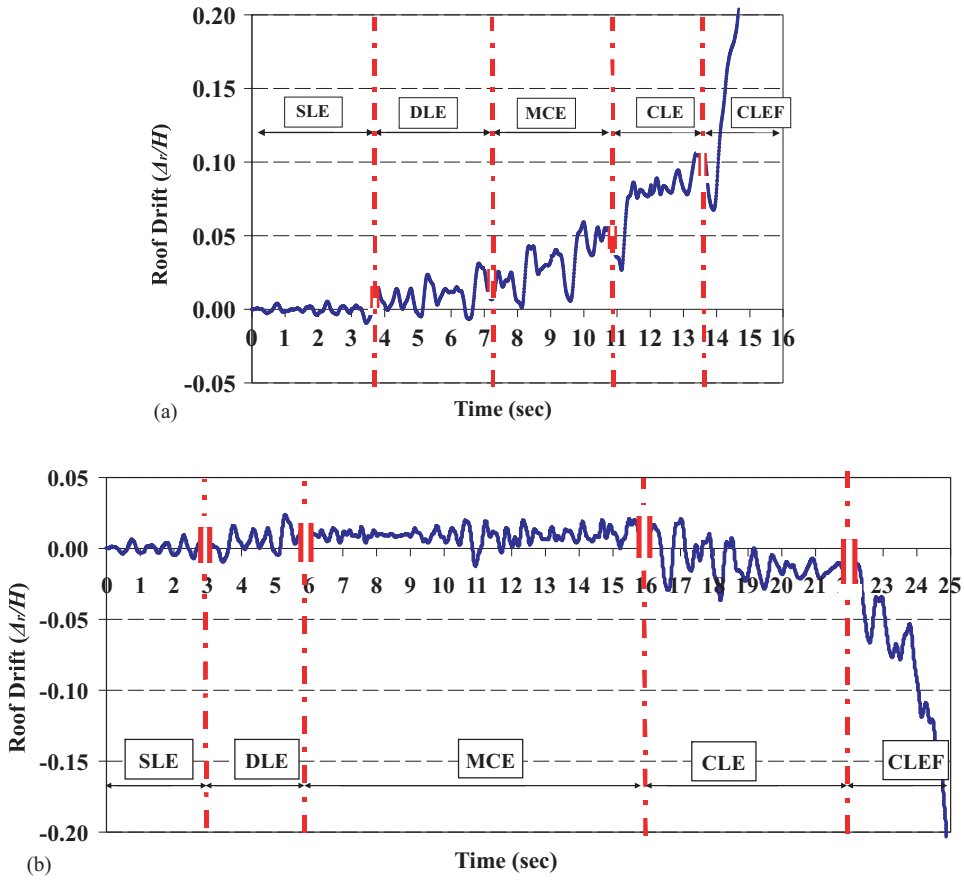

Figure 9. History of roof drift angle for Frames 1 and 2 at various ground motion intensities: (a) Frame 1 and (b) Frame 2.

For Frame 1 the test series produces incremental increases in roof drift of the same sign. The CLE intensity test produces a maximum roof drift angle of 0.11 compared with the pre-Buffalo prediction of 0.17. Although the difference of 0.06 may appear significant, the frame was at the point of incipient collapse because when the intensity scale factor was increased from 1.9 to 2.2 (the CLEF intensity test), the frame collapsed during the first inelastic excursion in the direction of the residual drift from CLE (see Figure 9(a)). The ground motion scale factor for the CLEF test is 2.2, but a much smaller scale factor would also have led to collapse as demonstrated later in the post-Buffalo predictions.

For Frame 2, the pre-Buffalo predictions indicate that the frame should be close to collapse after the MCE intensity test. However, as seen in Figures 7(b) and 9(b), the MCE test was benign and did not lead to an increase in the roof drift. It was found out after completion of the test series that the input motion to the earthquake simulator was only about one-half that of the target motion, which invalidated the pre-Buffalo response predictions. The authors reverted to the CP record for further testing and imposed this record with a scale factor of 2.2 to bring the structure close to collapse. However, this test reversed the sign of the residual drift and a small drift remained after the test as seen in Figures 7(b) and 9(b). This significant change in the behavior demonstrates the sensitivity of the response to relatively small differences in the initial conditions. For Frame 1, shaking with a scale factor of 1.9 led to very large residual drifts, whereas for Frame 2 the residual drifts for shaking with a scale factor of 2.2 were small even though the initial conditions before the execution of the tests were similar. The measured residual drifts in both frames before and after the CLE tests are shown in Figure 10 together with analytical predictions based on the post-Buffalo numerical model.

DOI: 10.1002/eqe

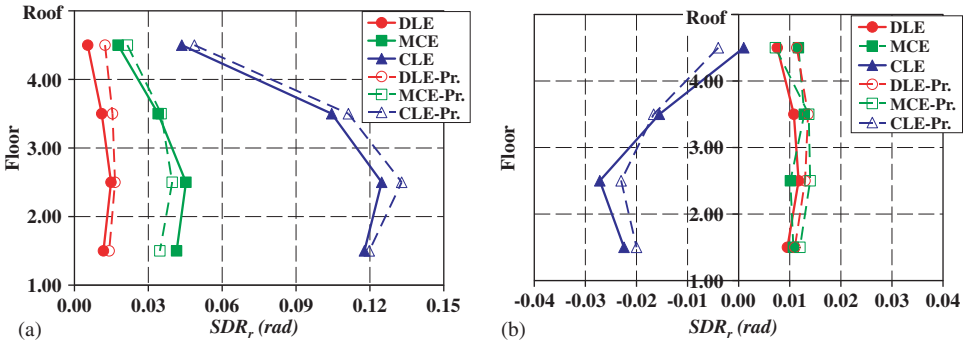

Figure 10. Residual story drifts for Frames 1 and 2: (a) Frame 1 and (b) Frame 2.

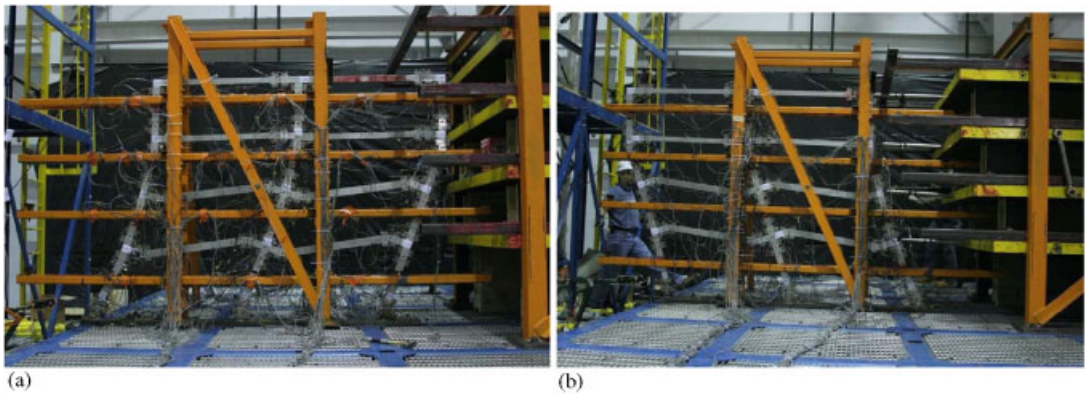

Figure 11. Collapse mechanisms after the completion of collapse earthquake simulator tests: (a) Frame 1 and (b) Frame 2.

The test series for Frame 2 was completed by applying an additional test with a scale factor of 2.2 (denoted as the CLEF test). As seen in Figure 9(b), several large inelastic excursions occurred before the frame collapsed in the direction opposite to that of Frame 1.

Figure 11 shows the collapse mechanisms for the two test frames. In both cases the mechanism extends over three stories and consists of plastic hinging at the ends of the beams of the lower two floors and in the columns at the base of the frame and the top of the third story. The upper portion of the mechanism is formed by column plastic hinges at the top of the third story although the strong column–weak beam criterion was met in the design of the prototype frame. This observation confirms that meeting the strong column–weak beam criterion does not prevent the formation of plastic hinges in columns because of changes in the moment diagram in the inelastic range of behavior [34]. Another reason for the column hinging is the third story column splice and the use of a weaker column above the splice. To avoid a column plastic hinge at the top of 3rd story columns, the capacity of the column would have to be nearly doubled, based on analytical simulations in which the third story column strength is increased till the collapse mechanism is changed to a complete 4-story mechanism.

8.3. Peak story drift ratios

The peak story drift ratios (SDRs) are presented in Figure 12 for the different intensities of ground motion. For both test frames the largest drifts are associated with the CLEF test at the time instant before the frame impacts the safety system (shown as the incipient collapse level, ICL, in the figure legends). The largest SDRs occur in the bottom two stories. The SDRs are computed using the Krypton system.

DOI: 10.1002/eqe

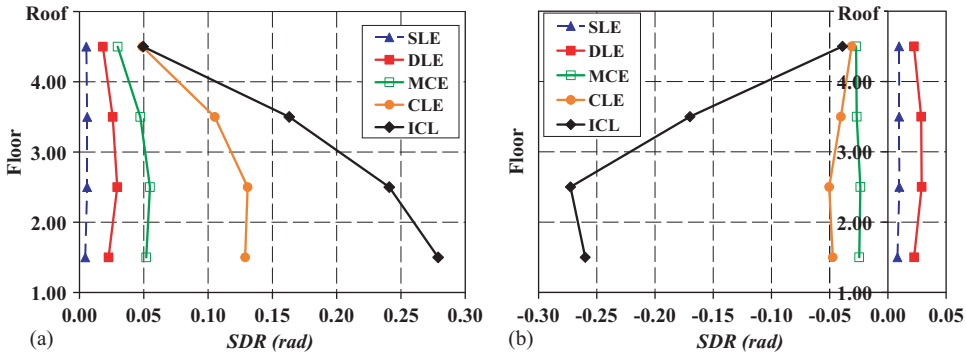

Figure 12. Peak SDRs at various ground motion intensities for both frames: (a) Frame 1 and (b) Frame 2.

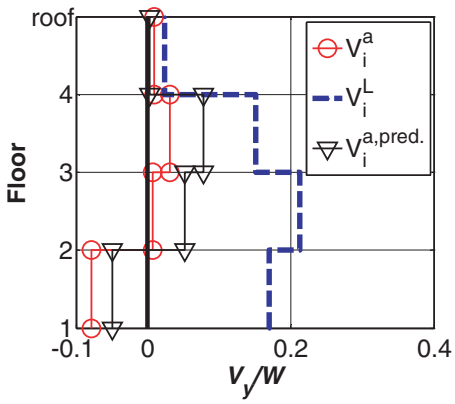

Figure 13. Story shear forces of Frame 1 at $t=7.00$ s during CLEF ground motion intensity together with post-test prediction.

8.4. *Story shear distributions*

Story shear forces are usually defined as the sum of inertial forces above a certain story. This definition implies that $P-\Delta$ effects, which amplify member forces and story drifts, are considered separately from inertia forces. In the earthquake simulator tests both the inertia forces and the $P-\Delta$ effects are transferred through the horizontal links from the mass simulator to the test frame. In the following discussion we distinguish between two types of story shear forces; those generated by inertia forces and those generated by inertia forces plus $P-\Delta$ effects, referred to here as *effective* story shear forces. The former are measured as the sum of products of the mass of the mass-simulator floor plate and the absolute acceleration, and the latter are measured as the sum of the link forces transferred from the mass simulator to the essentially weightless test frame. The difference between the two quantities is due to the $P-\Delta$ effect. Transferring $P-\Delta$ effects through links from the mass simulator to the test frame involves the same approximations as are made in an analytical model in which $P-\Delta$ effects are simulated through a leaning column. This involves the assumption that the moment diagram in all elements due to $P\cdot\delta$ is identical to that caused by $V'\cdot h$, where P is the total vertical load tributary to the frame, δ is the story displacement, V' is an equivalent story shear force, and h is the height of the story under consideration. This assumption is approximate but has been found to have only a very small effect on the seismic response of frame structures in the inelastic range [35].

Figure 13 shows the distribution of story shear forces along the height of the structure measured at $t=7$ s from the beginning of CLEF, for both inertia based shear forces (denoted as V_i^a) and effective shear forces based on link forces (denoted as V_i^L) together with analytically predicted shear forces (including $P-\Delta$) based on post-test predictions (denoted as $V_i^{\text{a,pred.}}$). The difference

DOI: 10.1002/eqe

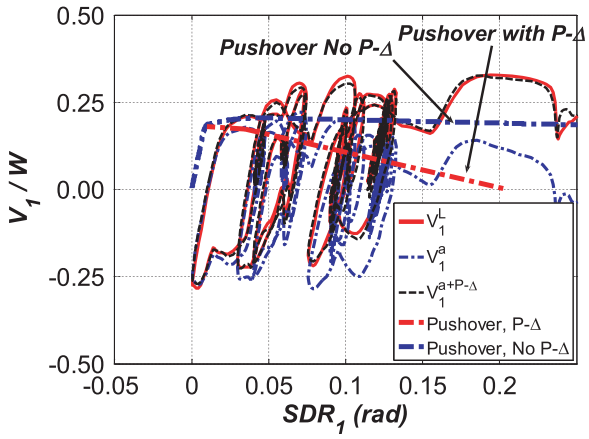

Figure 14. Base shear–first story drift relationship for Frame 1 through collapse (CLE and CLEF tests).

between the inertia-based and effective story shear forces is due to $P-\Delta$ effects. Similar results are observed for Frame 2. A detailed description of force and overturning moment distributions along the height of both frames is presented in Lignos and Krawinkler [22].

8.5. *Quantification of $P-\Delta$ effects*

The test setup, with an essentially weightless test frame driven by a mass simulator, provides a unique opportunity to measure $P-\Delta$ effects up to collapse. Figure 14 shows the relationship between first SDR and normalized base shear for Frame 1 up to collapse. The thin solid curve is the *effective* base shear as obtained from the horizontal links (V_1^L) connecting the mass simulator to the test frame. This shear force includes $P-\Delta$ effects. The thin dashed-dotted curve is the inertia based base shear obtained by summing the products of floor mass and the corresponding absolute acceleration ($=V_1^a$).

For a given drift, the $P-\Delta$ effect in the first story can be approximated by an equivalent story shear equal to $P\delta_1/h_1$, where P is the total weight of the plates of the mass simulator, h_1 is the height of the first story, and δ_1 is the drift in the first story. When $P\delta_1/h_1$ is added toV_1^a, the dashed curve in Figure 14 is obtained. This curve is close to the V_1^L versus the measured drift relationship and confirms that the $P-\Delta$ effect can be represented reasonably well by $P\delta/h$. Figure 14 also shows that the inertia-based shear force approaches zero at an SDR of about 0.15, which means that the test frame plus mass simulator would collapse if the ground motion would stop at this time instant, because the $P-\Delta$ effect fully offsets the lateral resistance of the frame. The observed large increase in the lateral resistance of the scale model at story drifts larger than 0.15 is due to the reversal of the ground motion of the earthquake simulator.

Also shown in Figure 14, with thick dashed-dotted lines, are the base shear–first story drift relationships obtained from the pushover analysis with and without second-order effects. A comparison of these curves with envelopes of the dynamic test results provides an insight into the value of the pushover analysis for response prediction for a first mode-controlled frame structures. The yield base shear force and effect of $P-\Delta$ on the behavior of the frames prior to collapse are simulated fairly well. The collapse mechanism for both frames is also predicted correctly. However, the pushover curves are unable to simulate the dynamic amplification of the base shear due to ground motion reversals, particularly near collapse. The maximum dynamic story shear force is about 50% larger than predicted by the static (pushover) analysis.

9. RESPONSE PREDICTIONS

A direct comparison of the maximum roof drifts obtained from the pre-Buffalo response predictions and the earthquake simulator tests for different ground motion intensities were provided in Figure 7

DOI: 10.1002/eqe

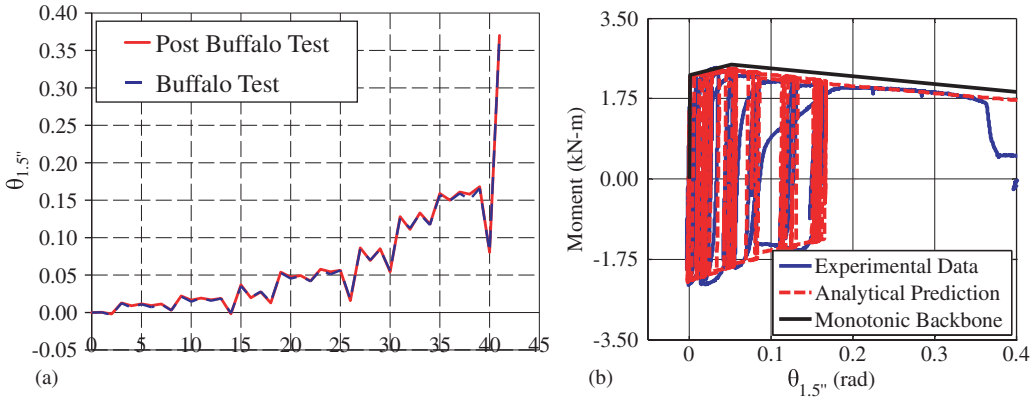

Figure 15. Post-Buffalo component test: (a) rotation history of plastic hinge element at base of exterior column of Frame 1 and (b) moment–rotation diagram obtained from component test and model calibration.

for both frames. For Frame 2 though only results at and below the DLE level can be compared with pre-Buffalo test predictions for reasons given in Section 8.2. These predictions are based on models developed using the data from the pre-Buffalo component tests as summarized in Table I, in which the specimens are subjected to symmetric cyclic loading histories of the type specified in AISC [26]. An important observation from the earthquake simulator tests is that the symmetric cyclic loading is not representative of demands on components in framing systems close to collapse and when $P-\Delta$ effects control the response. This observation, prompted the authors to undertake a post-Buffalo testing program in which representative components of the test frames are subjected to the loading history measured in the earthquake simulator tests.

9.1. Post-buffalo component experiments of the four most critical plastic hinge regions

The clip gages attached to each plastic hinge element provided plastic hinge rotation histories for each earthquake simulation. This information was used to derive displacement histories for post-Buffalo tests of the first four of the five most critical plastic hinge regions, which were performed using the test setup shown in Figure 5(b).

Figure 15(a) shows the rotation history experienced by the plastic hinge element at the first floor exterior beam (F2B1R) of Frame 1 for the full series of dynamic tests from SLE to CLEF. This history shows a clear drifting to one side and has no resemblance to the symmetric loading histories executed in the pre-Buffalo component tests. Superimposed (but hardly visible) is the rotation history experienced by the plastic hinge element in the post-Buffalo component experiment. The two rotation histories are almost identical, indicating confidence in the reproduction of the earthquake simulator test rotation histories in the component tests.

Figure 15(b) presents the moment-rotation diagram obtained from the post-Buffalo component test using the loading history given in Figure 15(a). Superimposed is the modified IK deterioration model after calibration [22]. The modeling parameters obtained from the post-Buffalo test series, which focused on the four out of five most critical locations of the test frames, are summarized in Table II. A comparison of the deterioration parameters summarized in Tables I and II shows that the major difference between the pre-Buffalo and post-Buffalo results is in θ_{pc} values, which are clearly larger in the post-Buffalo calibrations. A difference is also noted in θ_p values for C1S3T and F4B1R locations.

The main reason for the difference in θ_p and θ_{pc} values is the effect of loading history. The values of θ_{pc} obtained from the model plastic hinge elements are larger than those from the prototype-reduced beam sections because lateral torsional buckling is not captured in the plastic hinge elements. However, the observation that the symmetric cyclic loading leads to low values of θ_{pc} holds true in both the model and prototype domains. The smaller difference between the θ_{pc} values of the F2B1R location for pre- and post-Buffalo test component experimentation

DOI: 10.1002/eqe

Table II. Component modeling parameters for post-Buffalo collapse prediction.

Location	Width w (cm)	M_y (kN m)	K_e (kN m/rad)	M_c/M_y	θ_p (rad)	θ_{pc} (rad)	Λ	κ
C1S1B*	3.40	3.73	2924	1.10	0.050	2.00	1.30	0
C1S1T†	2.80	3.06	2331	1.10	0.050	2.00	1.30	0
C1S3T‡	1.47	1.61	1265	1.08	0.055	2.40	1.00	0
F2B1R§	2.11	2.15	1469	1.10	0.050	1.60	1.80	0
F4B1R¶	1.47	1.50	1265	1.08	0.055	2.40	1.00	0

Refer Table I for footnotes.

compared to the other locations summarized in Tables I and II is attributed to the fact that for F2B1R a monotonic curve was used to obtain the θ_p and θ_{pc} values for pre-Buffalo test predictions. For the other plastic hinge elements only cyclic tests were available. The monotonic curve for the F2B1R plastic hinge location is comparable with the unidirectional loading shown in Figure 15(b).

In general, the θ_p values for RBS and non-RBS components are not expected to have the same magnitude. However, for the sections of the prototype structure discussed in Section 4 the θ_p values of all the components shown in Figure 2(b) have a similar magnitude as determined from a recently developed database for component deterioration of steel beams and columns [22, 23], i.e. for simplicity, the unbraced length (see Figure 4(b), L_t, L_b) in all steel plates of the plastic hinge locations of the model structure is kept the same.

9.2. Post-buffalo response predictions

The purpose of the post-Buffalo response predictions is to investigate whether more accurate response predictions can be obtained by modifying the analytical model based on the component modeling parameters obtained from the post-Buffalo component tests. The recorded earthquake simulator motions are used in these predictions and the friction damping in the rod-ends is included in the analysis with the use of a friction element (see [22]).

A comparison of deterioration parameters from Tables I and II shows that values of plastic rotation capacity are essentially identical. The rates of cyclic deterioration (Λ) of the beams are somewhat different. In a study by Ibarra and Krawinkler [10] it was shown that variations in this parameter of the magnitude seen here do not have a significant effect on the collapse capacity of deteriorating structural systems.

The values of θ_{pc} based on the post-Buffalo component tests are clearly larger than those of the pre-Buffalo tests for reasons discussed previously. A smaller θ_{pc} value amplifies the effect of $P-\Delta$ on the collapse capacity of a frame structure: the structure deflects more due to $P-\Delta$ and collapse occurs earlier. Hence, only the differences in θ_{pc} have a significant effect on the response of the test frame during MCE and higher intensities of shaking.

Figure 16 shows the IDA curves for both scale models, as obtained from the earthquake simulator tests and the post-Buffalo analytical predictions. The global response of both models is predicted well with the use of relatively simple analytical models if the chosen values of the deterioration parameters are robust. The dashed-dotted line in Figures 16(a) and (b) beyond the CLE intensity of shaking indicates that both frames would have collapsed under shaking with a smaller scale factor than 2.2.

Figure 17 shows a time window of the first story drift histories obtained from the CLE and CLEF earthquake simulator tests for Frame 1 together with the response from the post-Buffalo simulations. The analytical prediction is accurate.

The conclusion is that the physical models (the two 1:8 scale test frames) and the post-Buffalo analytical models are essentially equivalent. But this equivalence is achieved only through improvements of the analytical models based on component tests performed after the earthquake simulator tests. Reliable collapse predictions necessitates (a) the availability of a versatile component model capable of replicating random cyclic response and all important deterioration modes associated

DOI: 10.1002/eqe

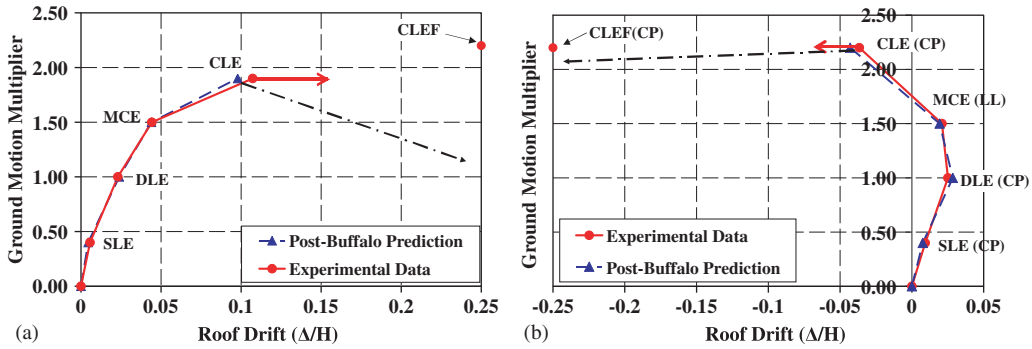

Figure 16. IDAs for both scale models based on post-Buffalo predictions and experimental data: (a) Frame 1 and (b) Frame 2.

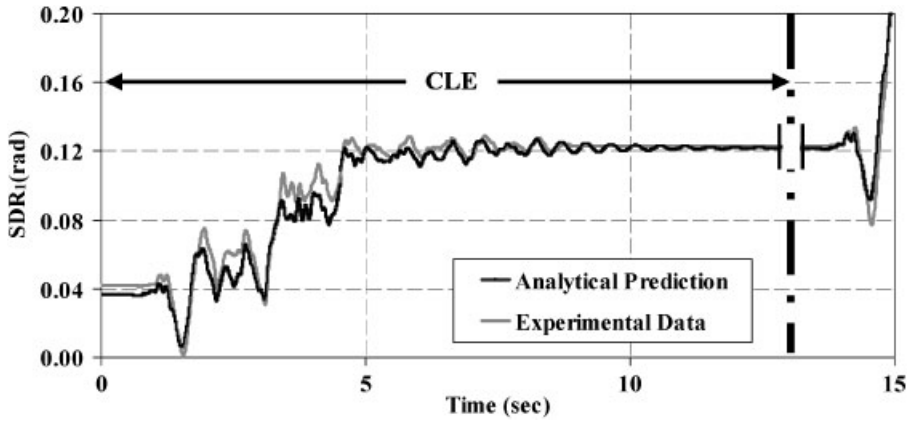

Figure 17. History of first SDR of Frame 1 based on the post-Buffalo predictions and experimental data for the CLE and CLEF intensities of shaking.

with it, and (b) the availability of experimental data from which accurate values of modeling parameters can be obtained.

10. SUMMARY AND CONCLUSIONS

The analytical and physical simulations of the earthquake response of two 1:8 scale models of a code-compliant, two-bay steel moment-resisting frame are described through collapse. The two models were subjected to a series of ground motions on the NEES earthquake simulator at the University at Buffalo. The test series performed on each model is a 'physical' incremental dynamic analyses with non-zero initial conditions. The earthquake simulator tests produced a comprehensive set of data that quantifies demand parameters such as story forces and shears, story drifts, plastic rotations, and floor accelerations, in the elastic and inelastic ranges through collapse. The response histories and metadata are available through the NEES repository (http://nees.org/resources/723). As the models are of a bare steel frame only, and important factors contributing to collapse could not be addressed, the results must be used with care for collapse predictions of buildings constructed with steel moment-resisting frames.

The collapse mechanism of both models involves three stories of framing. In both frames, plastic hinges form at the top of the third story columns even though the prototype structure fulfilled the strong column–weak beam criterion at these locations. The two frames collapse in different directions because different ground motion sequences are employed.

DOI: 10.1002/eqe

The instrumented links between the mass simulator and model enabled the authors to quantify $P-\Delta$ effects. The $P-\Delta$ effect in the first story is represented well from elastic response through collapse by an equivalent story shear equal to $P\delta_1/h_1$, where P is the total weight of the mass simulator plates, h_1 is the height of the first story, and δ_1 is the drift in the first story.

Relatively simple analytical models can be used to predict the behavior of moment frames up to collapse, provided that the deterioration characteristics of critical components are adequately represented in the analytical models. An accurate representation of the post-capping rotation capacity is essential for the prediction of collapse capacity.

The use of symmetric cyclic loading protocols for component testing provides insufficient information for component deterioration modeling near collapse. Alternative loading protocols are needed. A protocol in which relatively small inelastic cycles are followed by unidirectional loading to extreme deformations, or a cyclic test supplemented with a monotonic test would provide more relevant information for the purpose of developing robust component deterioration models for collapse predictions.

ACKNOWLEDGEMENTS

This study is based on the work supported by the United States National Science Foundation (NSF) under Grant No. CMS-0421551 within the George E. Brown, Jr. Network for Earthquake Engineering Simulation Consortium Operations. The financial support of NSF is gratefully acknowledged. The authors also thank REU students Mathew Alborn, Melissa Norlund and KarHim Chiu and the technical staff at the NEES facility at the University at Buffalo for their assistance with many aspects of the earthquake-simulator testing program. Any opinions, findings, and conclusions or recommendations expressed in this paper are those of the authors and do not necessarily reflect the views of NSF.

REFERENCES

1. Foliente G. Hysteresis modeling of wood joints and structural systems. *Journal of Structural Engineering* (ASCE) 2000; **121**(6):1013–1022.
2. Bouc R. Forced vibration of mechanical systems with hysteresis. *Proceedings of 4th Conference on Nonlinear Oscillations*, Prague, Portugal, 1967; 315.
3. Wen Y-K. Equivalent linearization for hysteretic systems under random excitation. *Journal of Applied Mechanics* 1980; **47**:150–154.
4. Baber T, Noori MN. Random vibration of degrading, pinching systems. *Journal of Engineering Mechanics* (ASCE) 1985; **111**(8):1010–1026.
5. Reinhorn AM, Madan A, Valles RE, Reichmann Y, Mander JB. Modeling of masonry infill panels for structural analysis. *Report NCEER-95-0018*, State University of New York at Buffalo, Buffalo, NY, 1995.
6. Sivaselvan M, Reinhorn AM. Hysteretic models for deteriorating inelastic structures. *Journal of Engineering Mechanics* (ASCE) 2000; **126**(6):633–640.
7. Iwan WD. A distributed-element model for hysteresis and its steady-state dynamic response. *Journal of Applied Mechanics* 1966; **33**(42):893–900.
8. Mostaghel N. Analytical description of pinching, degrading hysteretic systems. *Journal of Engineering Mechanics* (ASCE) 1999; **125**(2):216–224.
9. Ibarra LF, Medina RA, Krawinkler H. Hysteretic models that incorporate strength and stiffness deterioration. *Earthquake Engineering and Structural Dynamics* 2005; **34**(12):1489–1511.
10. Ibarra LF, Krawinkler H. Global collapse of frame structures under seismic excitations. *Report No. PEER 2005/06*, Pacific Earthquake Engineering Research Center (PEER), University of California, Berkeley, 2005.
11. Zareian F, Krawinkler H. Simplified performance based earthquake engineering. *Report No. TB 169*, The John A. Blume Earthquake Engineering Center, Department of Civil and Environmental Engineering, Stanford University, 2006.
12. Haselton CB, Deierlein GG. Assessing seismic collapse safety of modern reinforced concrete moment frame buildings. *Report No. TR 156*, The John A. Blume Earthquake Engineering Center, Department of Civil and Environmental Engineering, Stanford University, 2007.
13. Vian D, Bruneau M. Experimental investigation of P-Delta effects to collapse during earthquakes. *Report MCEER-01-0001*, 2001.
14. Vian D, Bruneau M. Tests to structural collapse of single degree of freedom frames subjected to earthquake Excitations. *Journal of Structural Engineering* (ASCE) 2003; **129**:1676–1685.
15. Kanvinde AM. Methods to evaluate the dynamic stability of structures-shake table tests and nonlinear dynamic analyses. *Earthquake Engineering Research Institute* (*EERI*) *Paper Competition Winner*, *Proceedings of EERI Meeting*, Portland, Oregon, February 2003.

DOI: 10.1002/eqe

16. OpenSees. Open System for Earthquake Engineering Simulation. *Pacific Earthquake Engineering Research Center* (*PEER*). Available from: http://opensees.berkeley.edu), 2009.
17. Rodgers J, Mahin S. Effects of connection fractures on global behavior of steel moment frames subjected to earthquakes. *Journal of Structural Engineering* (ASCE) 2006; **132**(1):78–88.
18. Suita K, Yamada S, Tada M, Kasai K, Matsuoka Y, Sato E. Results of recent E-Defense tests on full-scale steel buildings: part 1—collapse experiment on 4-story moment frame. *Proceedings Structures Congress* ASCE, Vancouver, 2008.
19. Suita K, Yamada S, Tada M, Kasai K, Matsuoka Y, Shimada Y. Collapse experiment on 4-story steel moment frame: part 2 detail of collapse behavior. *Proceedings of 14th World Conference on Earthquake Engineering*, Beijing, China, 2008.
20. Tada M, Tamai H, Ohgami K, Kuwahara S, Horimoto A. Analytical simulation utilizing collaborative structural analysis system. *Proceedings of 14th World Conference on Earthquake Engineering*, Beijing, China, 2008.
21. Lignos DG, Krawinkler H, Zareian F. Modeling of component deterioration for collapse prediction of steel moment frames. *Proceedings*, *Behavior of Steel Structures in Seismic Areas*, STESSA, Philadelphia, PA, 2009.
22. Lignos DG, Krawinkler H. Sidesway collapse of deteriorating structural systems under seismic excitations. *Report No. TR 172*, The John A. Blume Earthquake Engineering Center, Department of Civil and Environmental Engineering, Stanford University, 2009.
23. Lignos DG, Krawinkler H. A database in support of modeling of component deterioration for collapse prediction of steel frame structures. *Proceedings of ASCE Structures Congress*, Long Beach, CA, SEI Institute, 2007.
24. Gupta A, Krawinkler H. Prediction of seismic demands for SMRFs with ductile connections and elements. *Report No. SAC/BD-99/06*, SAC Background Document, 1999.
25. IBC. International building code. *International Code Council*, Birmingham, AL, 2003.
26. AISC, Seismic provisions for structural steel buildings, including supplement No. 1. American Institute of Steel Construction, Inc. Chicago, IL, 2005.
27. SAC Joint Venture. Recommended seismic design criteria for new steel moment frame buildings. *Report No. FEMA 350*, Federal Emergency Management Agency, Washington, DC, 2000.
28. Moncarz PD, Krawinkler H. Theory and application of experimental model analysis in earthquake engineering. *Report No. 50*, The John A. Blume Earthquake Engineering Center, Department of Civil Engineering, Stanford University, 1981.
29. Uang CM, Yu K, Gilton C. Cyclic response of RBS moment connections: loading sequence and lateral bracing effects. *Report No. SSRP-99/13*, Department of Structural Engineering, UCSD, 2000.
30. Prakash V, Powell GH, Campbell S. DRAIN-2DX: basic program description and user guide. *Report No. UCB/SEMM-1993/17*, University of California, Berkeley, CA, 1993; 97.
31. Vamvatsikos D, Cornell CA. Incremental dynamic analysis. *Earthquake Engineering and Structural Dynamics* 2002; **31**(3):491–514.
32. Bracci JM, Reinhorn AM, Mander JB. Seismic resistance of reinforced concrete frame structures designed only for gravity loads: part III—experimental performance and analytical study of a structural model. *Report NCEER-92-0029*, National Center for Earthquake Engineering Research, University at Buffalo, 1992.
33. Lignos DG, Krawinkler H, Whittaker AS. Collapse assessment of a 4-story steel moment resisting frame. *Proceedings of 2nd International Conference on Computational Methods in Structural Dynamics and Earthquake Engineering*, *CompDyn 2009*, Rhodes, Greece, 22–24 June 2009.
34. Krawinkler H. Importance of good nonlinear analysis. *The Structural Design of Tall and Special Buildings* 2006; **15**:515–531.
35. Adam C, Krawinkler H. Large displacement effects on seismically excited elastic–plastic frame structures. *Asian Journal of Civil Engineering* 2004; **5**(12):41–55.

DOI: 10.1002/eqe